Phys Chem Minerals (2011) 38:407–417
DOI 10.1007/s00269-010-0414-z

ORIGINAL PAPER

Thermal equation of state of $CaIrO_3$ post-perovskite

Wei Liu · Matthew L. Whitaker · Qiong Liu · Liping Wang · Norimasa Nishiyama · Yanbin Wang · Atsushi Kubo · Thomas S. Duffy · Baosheng Li

Received: 14 June 2010 / Accepted: 6 December 2010 / Published online: 8 January 2011

Abstract The pressure–volume–temperature (P–V–T) relation of $CaIrO_3$ post-perovskite (ppv) was measured at pressures and temperatures up to 8.6 GPa and 1,273 K, respectively, with energy-dispersive synchrotron X-ray diffraction using a DIA-type, cubic-anvil apparatus (SAM85). Unit-cell dimensions were derived from the Le Bail full profile refinement technique, and the results were fitted using the third-order Birth-Murnaghan equation of state. The derived bulk modulus K_{T0} at ambient pressure and temperature is 168.3 ± 7.1 GPa with a pressure derivative $K'_{T0} = 5.4 \pm 0.7$. All of the high temperature data, combined with previous experimental data, are fitted using the high-temperature Birch-Murnaghan equation of state, the thermal pressure approach, and the Mie-Grüneisen-Debye formalism. The refined thermoelastic parameters for $CaIrO_3$ ppv are: temperature derivative of bulk modulus $(\partial K_T/\partial T)_P = -0.038 \pm 0.011$ GPa K^{-1}, $\alpha K_T = 0.0039 \pm 0.0001$ GPa K^{-1}, $(\partial K_T/\partial T)_V = -0.012 \pm 0.002$ GPa K^{-1}, and $\left(\partial^2 P/\partial T^2\right)_V = 1.9 \pm 0.3 \times 10^{-6}$ GPa^2 K^{-2}. Using the Mie-Grüneisen-Debye formalism, we obtain Grüneisen parameter $\gamma_0 = 0.92 \pm 0.01$ and its volume dependence $q = 3.4 \pm 0.6$. The systematic variation of bulk moduli for several oxide post-perovskites can be described approximately by the relationship $K_{T0} = 5406.0/V(\text{molar}) + 5.9$ GPa.

Keywords $CaIrO_3$ post-perovskite · Thermal equation of state · High pressure and high temperature

W. Liu (✉) · M. L. Whitaker · Q. Liu · L. Wang · B. Li
Mineral Physics Institute,
Stony Brook University, Stony Brook, NY 11794, USA
e-mail: weiliu3@notes.cc.sunysb.edu

M. L. Whitaker · N. Nishiyama
Geodynamics Research Center, Ehime University,
Bunkyo-cho 2-5, Matsuyama 790-8577, Japan

Y. Wang
Center for Advanced Radiation Sources,
University of Chicago, Chicago, IL 60637, USA

A. Kubo · T. S. Duffy
Department of Geosciences, Princeton University,
Princeton, NJ 08544, USA

Present Address:
Q. Liu
School of Earth and Space Sciences,
Peking University, 100871 Beijing, China

Present Address:
A. Kubo
Sumitomo Electric Hardmetal Corporation,
1-1-1 Koyakita, Itami, Hyogo 664-0016, Japan

Introduction

Experiments at high pressures and high temperatures and theoretical calculations have shown that, with increasing pressure, many compounds, e.g. (Mg, Fe)SiO_3, $MgGeO_3$, $MnGeO_3$, Fe_2O_3, Al_2O_3, Mn_2O_3, and $NaMgF_3$, will transform to the $CaIrO_3$-type post-perovskite (ppv) structure (Hirose et al. 2005; Murakami et al. 2004; Tateno et al. 2006; Caracas and Cohen 2005; Mao et al. 2004; Oganov and Ono 2004, 2005; Tsuchiya et al. 2005a; Ono and Ohishi 2005; Santillan et al. 2006; Martin et al. 2006). (Mg, Fe)SiO_3 perovskite (pv), the dominant lower-mantle phase, transforms to post-perovskite phase at around 120–125 GPa and above 2,000°C, which might correspond to the seismic anomalies observed in the D'' region (Panning and Romanowicz 2004; Hernlund et al. 2005; Lay et al. 2006;

Wookey et al. 2005). The physical and thermodynamic properties of post-perovskite are therefore important to explain the seismic anomalies at the core-mantle boundary (CMB) region. As a low-pressure analo of $MgSiO_3$-ppv, the thermodynamic properties of $CaIrO_3$ ppv under high pressures and high temperatures are of interest to the Earth sciences, although its applicability as an analo is not well established (Tsuchiya and Tsuchiya 2007; Kubo et al. 2008).

The $CaIrO_3$ structure can be visualized as isolated layers of IrO_6 octahedra normal to the *b* axis. The octahedra share edges along the *a*-axis and corners along the *c*-axis. Calcium occupies bi-capped trigonal prism sites between these layers (Rodi and Babel 1965). High-temperature drop calorimetry experiments showed a strongly positive Clapeyron slope for the phase boundary between perovskite and post-perovskite $CaIrO_3$ (Hirose and Fujita 2005). Hustoft et al. (2008) measured Raman Spectra of $CaIrO_3$ ppv up to 30 GPa. Lindsay-Scott et al. (2007) and Martin et al. (2007) reported thermal expansion results, determined by X-ray powder diffraction. Previous studies have also investigated the rheology, grain growth kinetics, and lattice preferred orientation of $CaIrO_3$ ppv (Miyajima et al. 2006; Miyajima and Walte 2009; Niwa et al. 2007; Walte et al. 2007; Yoshino and Yamazaki 2007; Miyagi et al. 2008; Hunt et al. 2009; Metsue et al. 2009). Equation of state (EoS) and elasticity of $CaIrO_3$ perovskite and post-perovskite phases have been studied experimentally only at high pressures and room temperature (Ballaran et al. 2007; Martin et al. 2007; Tsuchiya and Tsuchiya 2007), except for a single theoretical study using density functional theory (Stølen and Trønnes 2007). The absence of a thermal equation of state derived using high *P–T* experimental data highlights the need for further investigation of *P–V–T* data for this important material.

Unit-cell volume (*V*) measurements under simultaneous high pressure–temperature (*P–T*) conditions in large-volume presses using intense synchrotron X-rays have been one of the most useful ways to establish reliable thermal EoS for solids (e.g. Wang et al. 1996; Nishihara et al. 2004; Liu and Li 2006, Liu et al. 2008). In this paper, we report the results from in situ measurements of the unit-cell volumes of $CaIrO_3$ post-perovskite at simultaneous high *P–T* conditions to 8.6 GPa and 1,273 K, fully within the post-perovskite stability field as determined by Hirose and Fujita (2005). Thermoelastic parameters are derived from the current *P–V–T* data using various thermal equations of state, including the high-temperature Birch-Murnaghan EoS (e.g. Duffy and Wang 1998), the thermal pressure approach (e.g. Anderson 1995, 1999; Jackson and Rigden 1996), and the Mie-Grüneisen-Debye formalism (e.g. Jackson and Rigden 1996).

Experimental

The sample was prepared following the same procedure described by Miyagi et al. (2008). Polycrystalline $CaIrO_3$ ppv was synthesized from a 1:1 M ratio of CaO and IrO_2 by a two-step process. First, the mixture was heated in a vacuum-sealed silica tube at ambient pressure for 68 h at 1,250 K. The run products were composed of a mixture of oxides, $CaIrO_3$ perovskite, and post-perovskite. The sample was then compressed to 7 GPa and 1,370 K for 4 h in a large-volume apparatus at 13-ID-D station of the GSE-CARS sector of the Advanced Photon Source. This produced a sintered aggregate with dimensions of $\sim$1.5 mm in diameter and 1.9 mm long. X-ray diffraction confirmed that the sample was pure, homogeneous $CaIrO_3$ post-perovskite. A polycrystalline specimen of 0.8-mm long was cut, and both ends were polished to be flat. Bulk density of the specimen was determined to be 7.55 ± 0.01 g cm^{-3} using the Archimedes' immersion method, which was 92% of the theoretical X-ray density (8.22 g cm^{-3}) for $CaIrO_3$ ppv. The bench-top velocity measurement were performed on the $CaIrO_3$ ppv specimen and yielded $v_p = 5.71 \pm 0.03$ km s^{-1} and $v_s = 3.13 \pm 0.02$ km s^{-1}. The experimental equipment and its operation have been described in detail by Li et al. (2004).

The high-pressure, high-temperature experiments were performed using a DIA-type cubic-anvil apparatus (SAM85) installed at the superconducting wiggler beam line X17B2 of the National Synchrotron Light Source (NSLS) at Brookhaven National Laboratory (BNL). Details of this experimental set-up have been described elsewhere (Weidner et al. 1992; Kung et al. 2002; Li et al. 2004). The cube-shaped pressure medium was made of pre-compressed boron epoxy (4:1 wt% ratio), with an edge length of $\sim$6.4 mm. The polycrystalline specimen was embedded in a NaCl-BN powder mixture (10:1 wt% ratio), which provided a pseudo-hydrostatic environment for the specimen. The cell pressure was determined using the equation of state for NaCl (Decker 1971), and pressure uncertainties resulting from the measured NaCl cell parameters are about 0.2 GPa. Temperature was measured using W/Re3%-W/Re25% thermocouple wires placed immediately adjacent to the specimen (Li et al. 2004). The temperature variation between the sample/salt and the thermal couple is estimated to be less than 20 K (Wang et al. 1998).

In the current experiment, we first compressed the sample to 8.6 GPa at room temperature and then increased the temperature to $\sim$1,273 K. During decompression, 5 additional heating/cooling cycles were performed at fixed ram loads as shown in Fig. 1. To minimize the effect of non-hydrostatic stress built up during compression/decompression at room temperature, in each heating/

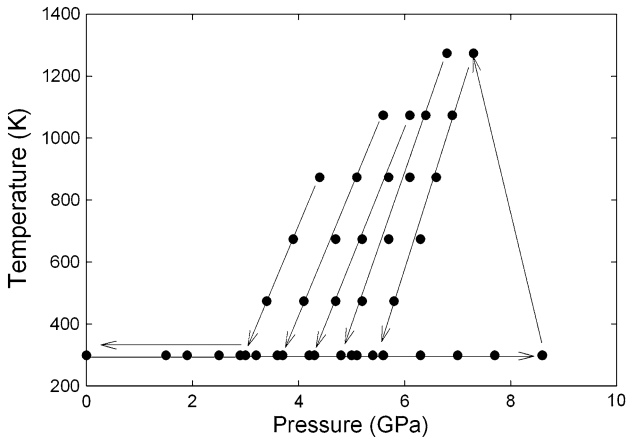

Fig. 1 Pressure–temperature path of experiments on post-perovskite $CaIrO_3$. Each point represents the *P–T* condition where the unit-cell volumes were measured. All of the data were collected in the stability field of post-perovskite phase according to Hirose and Fujita (2005)

cooling cycle, X-ray diffraction data were measured only during cooling (Wang et al. 1998). X-ray diffraction data from the specimen and the NaCl pressure standard were recorded in the energy dispersive mode using a Ge solid-state detector. The incident X-ray beam was collimated to 0.2 mm (horizontal) by 0.1 mm (vertical), and the diffraction angle was set at $2\theta = 6.532 \pm 0.002^{\circ}$. Final values of lattice parameters were obtained by Le Bail full profile fit (Le Bail 2005) using the software package GSAS (Larson and Von Dreele 2000) and the EXPGUI (Toby 2001), in which least-square fitting of the diffraction profile was achieved by the minimization of the difference between the observed and synthetic patterns.

Results and analysis

Unit-cell volumes of $CaIrO_3$ obtained along various isotherms from 298 to 1,273 K at pressures up to 8.6 GPa are listed in Table 1. X-ray diffraction patterns from the sample obtained at ambient conditions before and after the experiment are compared in Fig. 2 with major post-perovskite peaks indexed according to the *Pbnm* space group. No changes to the post-perovskite structure were observed within the resolution of the current data. The unit-cell volumes at ambient conditions (V_0) were determined to be 226.318 ± 0.037 and 226.270 ± 0.048 Å^3, respectively, before and after the experiment. They are in good agreement with the value of 226.3 ± 0.2 Å^3 reported by Hirose and Fujita (2005), but slightly smaller than the values of 226.3754 ± 0.0078 Å^3 reported by Martin et al. (2007), 226.38 ± 0.1 Å^3 from Ballaran et al. (2007), 226.402 ± 0.007 Å^3 from Lindsay-Scott et al. (2007), and 226.71 ± 0.23 from a single-crystal study (Sugahara et al. 2008). The isothermal compression at room temperature showed excellent agreement with the results of Ballaran et al. (2007) and Martin et al. (2007) in the current pressure range (Fig. 3).

We fit our room temperature *P–V* data with the following third-order Birch-Murnaghan EoS,

Table 1 Pressure, temperature, and unit-cell volume measurement of $CaIrO_3$ post-perovskite

P, GPa	*T*, K	*V(P,T)*, Å^3	ΔP_{th}, GPa
0.0	298	226.318 (37)	10^{-4}
2.5	298	222.994 (57)	10^{-4}
3.2	298	222.652 (63)	10^{-4}
3.7	298	221.880 (59)	10^{-4}
4.3	298	220.720 (60)	10^{-4}
5.0	298	220.440 (72)	10^{-4}
5.6	298	219.632 (71)	10^{-4}
6.3	298	218.708 (65)	10^{-4}
7.0	298	217.861(69)	10^{-4}
7.7	298	217.348 (73)	10^{-4}
8.6	298	216.563 (74)	10^{-4}
7.2	1,273	223.136 (75)	4.52
6.8	1,273	223.533 (58)	4.45
6.8	1,073	222.232 (67)	3.37
6.2	1,073	222.878 (39)	3.31
5.7	1,073	223.975 (63)	3.70
5.3	1,073	224.117 (53)	3.41
6.4	873	221.430 (68)	2.29
5.8	873	222.284 (59)	2.42
5.3	873	223.000 (57)	2.46
4.6	873	223.518 (53)	2.23
3.9	873	224.537 (63)	2.35
6.0	673	220.908 (59)	1.44
5.3	673	221.649 (68)	1.38
4.8	673	222.487 (56)	1.63
4.1	673	223.081 (63)	1.38
3.5	673	224.062 (57)	1.57
5.6	473	220.306 (62)	0.51
4.9	473	221.197 (59)	0.59
4.3	473	222.058 (49)	0.73
3.7	473	222.516 (57)	0.51
3.0	473	223.611 (56)	0.71
5.5	298	219.572 (58)	10^{-4}
4.7	298	220.763 (64)	10^{-4}
4.1	298	221.387 (53)	10^{-4}
3.4	298	222.131 (56)	10^{-4}
2.7	298	223.131 (49)	10^{-4}
1.7	298	225.133 (75)	10^{-4}
0.0	298	226.270 (48)	10^{-4}

Numbers in brackets are 1σ error in last digit(s)

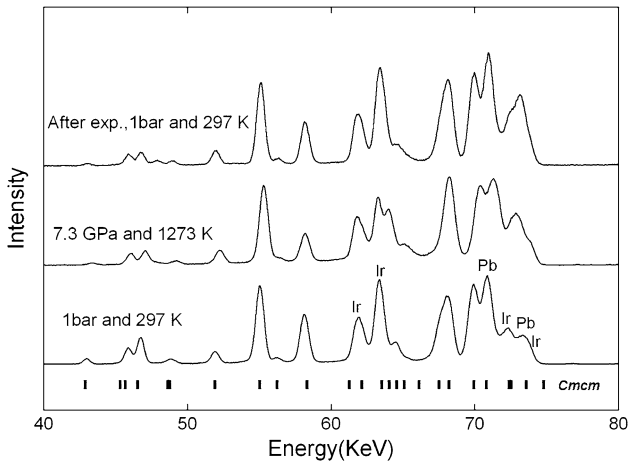

Fig. 2 Selected X-ray diffraction patterns for $CaIrO_3$ ppv at various *PT* conditions. The peaks marked by "Ir" and "Pb" are Ir and Pb fluorescence peaks

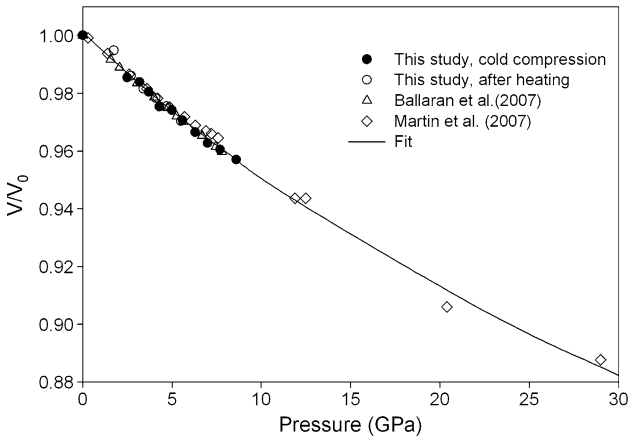

Fig. 3 Volume comparison from different studies for $CaIrO_3$ ppv at room temperature. Line is fitting results using the third-order Birch-Murnaghan equation of state ($K_{T0} = 168.3$ GPa and $K'_{T0} = 5.4$, and $V_0 = 226.566$ (181) Å^3

$$P(V,T) = \frac{3}{2}K_{T0}\left[\left(\frac{V_{T0}}{V}\right)^{7/3} - \left(\frac{V_{T0}}{V}\right)^{5/3}\right] \times \left\{1 + \frac{3}{4}\left(K'_{T0} - 4\right)\left[\left(\frac{V_{T0}}{V}\right)^{2/3} - 1\right]\right\} \quad (1)$$

where K_{T0}, K'_{T0}, and V_{T0} are isothermal bulk modulus, its pressure derivative, and the unit-cell volume at $T = 298$ K and ambient pressure, respectively. A least squares fitting of the present room T data to Eq. 1 yields $K_{T0} = 169.3 \pm 4.6$ GPa and $V_{T0} = 226.543 \pm 0.158$ Å^3, with an assumed $K'_{T0} = 4$. The value of K_{T0} is in good agreement with the theoretically calculated result of $K_{T0} = 164$ GPa with fixed $K'_{T0} = 4$ (Stølen and Trønnes 2007), but lower than the results of $K_{T0} = 181 \pm 3$ GPa reported by Ballaran et al. (2007) with a lower $K'_{T0} = 2.3$ and $K_{T0} = 180.2$ GPa by Martin et al. (2007) from a second-order Birch-Murnaghan EoS ($K'_{T0} = 4$) fitting, respectively. Considering that an increased compression range should help resolve the trade-off among K_{T0}, K'_{T0}, and V_{T0} and better constrain the three parameters, we combined our data with those obtained by Ballaran et al. (2007) and Martin et al. (2007) and fit the whole dataset to Eq. 1, yielding $K_{T0} = 168.3 \pm 7.1$ GPa, $K'_{T0} = 5.4 \pm 0.7$, and $V_{T0} = 226.566 \pm 0.181$ Å^3. For compatibility amongst the data from different studies, the volumes from these two studies were normalized to their respective starting values.

We applied three commonly employed methods to derive thermoelastic parameters from our current *P–V–T* data for $CaIrO_3$ ppv: (1) The high-temperature Birch-Murnaghan EoS (e.g. Saxena and Zhang 1990; Duffy and Wang 1998); (2) The thermal pressure approach (e.g. Anderson 1995, 1999; Jackson and Rigden 1996); and (3) The Mie-Grüneisen-Debye EoS (e.g. Jackson and Rigden 1996).

High-temperature Birch-Murnaghan EoS

Eq. 1 is used along various high-temperature isotherms at 473 K, 673 K, 873 K, 1,073 K and 1,273 K, respectively. Assuming that the second- and higher-order pressure derivatives of the bulk modulus are negligible, then K_{T0} and K'_{T0} are given by the properties at ambient conditions,

$$K_{T0} = K_0 + (\partial K_T/\partial T)_P(T - 298) \quad (2)$$

$$K'_{T0} = K'_0 \quad (3)$$

where K_0 and K'_0 are the isothermal values at ambient conditions. The temperature derivative of the bulk modulus $(\partial K_T/\partial T)_P$ is assumed to be constant throughout the whole temperature range. Zero-pressure unit-cell volume V_{T0}, at a given temperature T, is expressed as

$$V_{T0} = V_0 \exp \int_{298}^{T} \alpha_T \mathrm{d}T \quad (4)$$

$$\alpha_T = \alpha_0 + \alpha_1 T \quad (5)$$

where V_0 is the unit-cell volume at ambient conditions, and α_T is the thermal expansivity at ambient pressure and temperature T, empirically expressed by constant parameters, α_0, and α_1. Fitting the current *P–V–T* data (Table 1) to Eqs. 1–5, and fixing $K_{T0} = 168.3$ GPa, $K'_{T0} = 5.4$, and $V_{T0} = 226.566$ Å^3 as previously determined, we obtain a result of $(\partial K_T/\partial T)_P = -0.038 \pm 0.011$ GPa K^{-1}, $\alpha_0 = 1.48 \pm 0.16 \times 10^{-5}$ K^{-1} and $\alpha_1 = 2.40 \pm 0.54 \times 10^{-8}$ K^{-2}, with a root mean square (RMS) misfit of ~0.10 GPa. Our thermal expansion data derived from the high-temperature Birch-Murnaghan EoS analysis are in agreement with those of Lindsay-Scott et al. (2007) and

Martin et al. (2007) as shown in Fig. 4. The *P–V–T* fitting results and the measured $CaIrO_3$ ppv unit-cell volumes are plotted as a function of pressure in Fig. 5. Experimental data are reproduced quite well.

Thermal pressure approach

We also analyzed the *P–V–T* data using the thermal pressure approach (e.g. Anderson 1984; Jackson and Rigden 1996). The thermal pressure ΔP_{th} is obtained by subtracting the pressure at constant volume V and at room temperature from that measured at temperature T.

$$\Delta P_{th} = P(V,T) - P(V, 300\,\mathrm{K}) = \sum biXi(\eta, T) \tag{6}$$

where

$$\eta = V_0/V$$

$$X_1 = (T - T_0)\, b_1 = \alpha K_T, \tag{7}$$

$$X_2 = -(T - T_0) \ln \eta\, b_2 = (\partial K_T/\partial T)_V, \tag{8}$$

$$X_3 = (T - T_0)^2\, b_3 = \left(\partial^2 P/\partial T^2\right)_V/2, \tag{9}$$

with fixed $K_{T0} = 168.3$ GPa and $K'_{T0} = 5.4$, a fit of the current data to Eq. 6 gives $\alpha K_T = 0.0039 \pm 0.0005$ GPa K^{-1}, $(\partial K_T/\partial T)_V = -0.017 \pm 0.012$ GPa K^{-1}, and $\left(\partial^2 P/\partial T^2\right)_V = 2.2 \pm 0.4 \times 10^{-6}$ GPa^2 K^{-2}, with an RMS misfits of $\sim$0.17 GPa. Using the thermodynamic identity $(\partial K_T/\partial T)_P = (\partial K_T/\partial T)_V - \alpha K_T K'_T$, a value of -0.038 ± 0.013 GPa K^{-1} for $(\partial K_T/\partial T)_P$ is obtained, which is in excellent agreement with the result derived from the high-temperature Birch-Murnaghan EoS fit (Table 2). We also fit the combined high-temperature datasets including the study of Martin et al. (2007), and obtained $\alpha K_T = 0.0039 \pm 0.0001$ GPa K^{-1}, $(\partial K_T/\partial T)_V = -0.012 \pm 0.002$ GPa K^{-1},

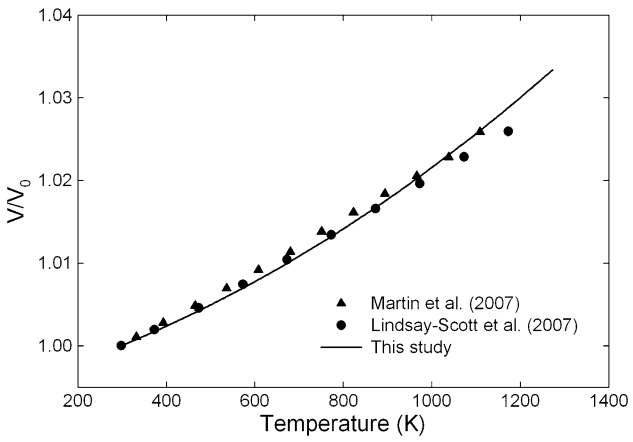

Fig. 4 Comparison of our thermal expansion data in the high-temperature Birch-Murnaghan EoS analysis with the thermal expansion data of Lindsay-Scott et al. (2007) and Martin et al. (2007)

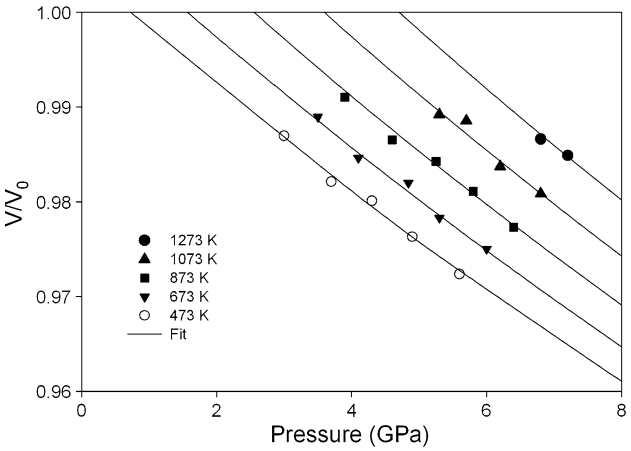

Fig. 5 High-temperature Birch-Murnaghan equation of state fit for $CaIrO_3$ ppv. Measured high-temperature unit-cell volumes (*symbols*) are showed. The errors of unit-cell volumes are less than the size of symbols

and $\left(\partial^2 P/\partial T^2\right)_V = 1.9 \pm 0.3 \times 10^{-6}$ GPa^2 K^{-2}, with an RMS misfits of $\sim$0.10 GPa. The value of $(\partial K_T/\partial T)_P$, using the new fitting results, is determined to be -0.033 ± 0.003 GPa K^{-1}, which is slightly lower that that derived from the high-temperature Birch-Murnaghan EoS approach. A comparison of the measured and fitted results is shown in Fig. 6.

Mie-Grüneisen-Debye formalism

In the Mie-Grüneisen-Debye equation of state, the thermal energy is approximated by the Debye lattice vibrational model, with only the acoustic modes taken into account (e.g. Jackson and Rigden 1996). The pressure $P(V,T)$ at a given volume and temperature can be expressed as the following forms:

$$P(V,T) = P(V,T_0) + \Delta P_{th} \tag{10}$$

with

$$\Delta P_{th} = \frac{\gamma(V)}{V}[E_{th}(V,T) - E_{th}(V,T_0)] \tag{11}$$

where subscript 0 refers to the principal isotherm (298 K). $P(V,T_0)$ is taken from Eq. 1. The thermal free energy E_{th} in Eq. 9 is calculated from the Debye model (Debye 1912), using

$$E_{th} = \frac{9nRT}{(\Theta/T)^3}\int_0^{\Theta/T} \frac{x^3 dx}{e^x - 1} \tag{12}$$

$$\Theta = \Theta_0 \exp[(\gamma_0 - \gamma)/q] \tag{13}$$

$$\gamma = \gamma_0 (V/V_0)^q \tag{14}$$

where n is the number of atoms per formula unit, R is the gas constant, Θ is the Debye temperature, γ_0 and Θ_0 are the

Table 2 Thermoelastic parameters derived from room-temperature and high-temperature Birch-Murnaghan (HTBM) EoS, thermal pressure (TP) approach and Mie-Grüneisen-Debye (MGD) formalism for $CaIrO_3$ ppv and comparison with the previous studies

Data	This study	This study + Ref. 1		This study	This study + Ref. 1 and Ref. 2	Ref. 1	Ref. 2	Ref. 3	Ref. 4
Methods	HTBM	TP	MGD	RTBM	RTBM	BM	BM		BM
K_{T0} *(GPa)*	*168.3*	*168.3*	*168.3*	169.3 (46)	168.3 (71)	180.2	181 (3)	144 (1)	164
K'_{T0}	*5.4*	*5.4*	*5.4*	*[4]*	5.4 (7)	–	2.3	4.8 (4)	*[4]*
$(\partial K_T/\partial T)_P$	−0.038 (11)	−0.033	–	–	–	–	–	–	–
α_0 ($\times 10^{-5}$K^{-1})	1.48 (16)	–	–	–	–	–	–	–	–
α_1 ($\times 10^{-8}$K^{-2})	2.40 (54)	–	–	–	–	–	–	–	–
αK_T	–	0.0039 (1)	–	–	–	–	–	–	–
$(\partial K_T/\partial T)_V$	–	−0.012 (2)	–	–	–	–	–	–	–
$\left(\partial^2 P/\partial T^2\right)_V (\times 10^{-6})$	–	1.9 (3)	–	–	–	–	–	–	–
q	–	–	3.4 (6)	–	–	–	–	–	–
Θ_0	–	–	*508*	–	–	–	–	–	–
γ_0	–	–	0.92 (1)	–	–	–	–	–	–
RMS misfit	0.10	0.10	0.12	0.22	0.36	–	–	–	–

Numbers in brackets are 1σ error in the last digits. Values in square brackets are assumed. Italic numbers indicate values being fixed. Thermal expansion $\alpha = \alpha_0 + \alpha_1 T$

K_{T0} and RMS misfit are in GPa; $(\partial K_T/\partial T)_P$, $(\partial K_T/\partial T)_V$, and αK_T are in GPa K^{-1}. $\left(\partial^2 P/\partial T^2\right)_V$ is in GPa^2 K^{-2}

Ref. 1: Martin et al. (2007); Ref. 2: Ballaran et al. (2007); Ref. 3 Lindsay-Scott et al. (2007); Ref. 4: Stølen and Trønnes (2007)

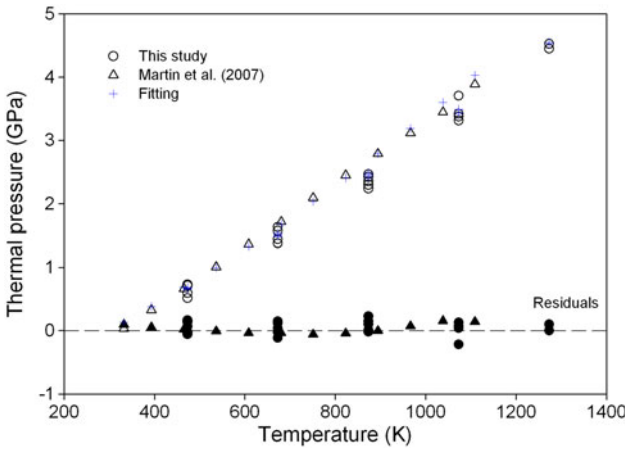

Fig. 6 A comparison of P_{th}(T)-P_{th}(298) for $CaIrO_3$ ppv and fitting results using thermal pressure approach as well as the residuals. The residuals are represented with *solid symbols* of the same shape as the corresponding experimental data

Grüneisen parameter and the Debye temperature at V_0, respectively, and $q = (d\ln\gamma/d\ln V)$ describes its volume dependence. The Debye temperature Θ is assumed to be a function of volume, and independent of temperature. Using the Mie-Grüneisen-Debye formalism, it is a common practice to fix Θ_0 during the fit using results from other techniques, such as acoustic measurement and/or calorimetric approach, because it cannot be well resolved in the fit compared to other parameters (e.g. Jackson and Rigden 1996).

The acoustic modes of lattice vibration are related to the compressional and shear wave velocities v_p and v_s, respectively. The acoustic Debye temperature Θ_{ac} is given by

$$\Theta_{ac} = \frac{h}{k}\left(\frac{3N}{4\pi}\right)^{\frac{1}{3}}\left(\frac{\rho}{M/p}\right)^{\frac{1}{3}} v_m \tag{15}$$

$$\frac{3}{v_m^3} = \frac{2}{v_s^3} + \frac{1}{v_p^3} \tag{16}$$

where M is the molecular mass; p is the number of atoms in the molecular formula; and k, h and N are Boltzmann's constant, Plank's constant, and Avogadro's number, respectively. Using the acoustic velocity data measured on the same sample ($v_p = 5.71$ km s^{-1}, $v_s = 3.13$ km s^{-1}, and $\rho = 7.55$ g cm^{-3} at ambient conditions), Θ_{ac0} is determined to be 450 K for the sample with a density equal to 92% theoretical density. Assuming the linear relationship between the velocities and porosity, the Debye temperature Θ_0 of a fully dense sample are estimated to be 508 K ($v_p = 6.28$ km s^{-1}, $v_s = 3.44$ km s^{-1}, and $\rho = 8.22$ g cm^{-3} at ambient conditions), which is much lower than the value of 703 ± 11 K calculated from internal energy via a Debye model (Lindsay-Scott et al. 2007).

The resulting best-fit Grüneisen parameter γ_0 and its volume dependence q for the dataset from this study are 0.99 (5) and 8.6 (35) at fixed $\Theta_0 = 508$ K. To examine how much the effect of the uncertainty of Debye

temperature on the fitting results, we performed a fit with $\Theta_0 = 550$ K and obtained a result of 1.00 ± 0.05 and 8.4 ± 3.5) for γ_0 and q, respectively. The RMS misfits for both fitting are ~0.15 GPa. It is evident that an uncertainty of 42 K in Θ_0 has negligible effect on the fitting results.

We also constrained q by combining our data with high-temperature results for $CaIrO_3$ ppv from previous studies (Martin et al. 2007). In this case, fitting the combined datasets to Eqs. 10–14 yielded 0.92 ± 0.01 and 3.4 ± 0.6 for γ_0 and q, respectively, with an RMS misfit of 0.12 GPa. It is clear that constraint on parameter q has been largely improved when the experimental data used in the fit covers a larger range of compression, since q is the volume dependence of γ (Shim and Duffy 2000). This has also been observed in our previous thermal equation of state study on San Carlos olivine (Liu and Li 2006). For a wide range of materials, Eq. 14 for the volume dependence of γ is shown to hold with $q = 1$ (e.g., Boehler and Ramakrishnan 1980; Stixrude and Bukowinski 1990). Fig. 7 shows the two combined datasets and fitting results as well as their respective residuals. Since fitting of the P–V–T data with this approach is insensitive to q away from unity, most of the previous fit have been carried out with q fixed at values between 0.5 and 1.5 for metals and minerals (e.g., Duffy and Ahrens 1995; Jackson and Rigden 1996); therefore, for ease of comparison, we fixed the value of $\Theta_0 = 508$ K and $q = 1$, and we obtained $\gamma_0 = 0.90 \pm 0.01$ with an RMS misfit of 0.14 GPa.

The values of γ_0 from all the above fittings are lower than those of 1.75 ± 0.08 from thermodynamic calculation and 1.66–1.80 from Raman spectroscopy study (Hustoft et al. 2008). It has been found that the γ of $CaGeO_3$ ppv decreases to 1.14–1.25 at 100 GPa and 4,000 K, from 1.75 at ambient conditions (Usui et al. 2010). Shim et al. (2007)

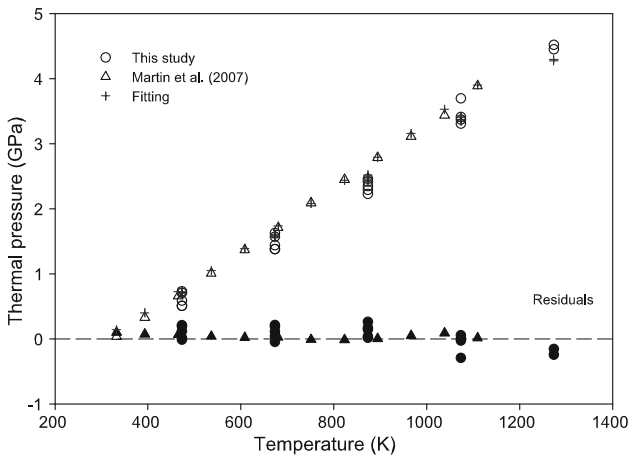

Fig. 7 The best-fitting Mie-Grüneisen-Debye models for the combined P–V–T datasets of $CaIrO_3$ ppv and residuals. The residuals are represented with *solid symbols* of the same shape as the corresponding experimental data

obtained $\gamma = 1.15 \pm 0.06$ at 65 GPa from the high-pressure Raman spectroscopic measurements. The γ of $Mg_{0.91}Fe_{0.09}SiO_3$ ppv was determined to be 0.79 ± 0.12 at 135 GPa and 2,300–2,700 K (Shim et al. 2008). It should be noted that the γ_0 obtained from the Mie-Grüneisen-Debye formalism fitting is an averaged value of $\gamma(V)$ through the volume range covered by the experimental data, instead of the γ_0 at $V = V_0$, which may result in a decreased γ in the current study.

The variation of bulk modulus for perovskite analos has been described approximately by the relationship $KV \approx$ constant (e.g., Liebermann et al. 1977; Bass 1984; Kung 1997; Liu et al. 2008). Liu et al. (2008) reexamined the systematic relationships between these isostructural analos and mantle silicate perovskites using updated elasticity data, and the relationship was determined to be $K_{S0} = 6{,}720/V(\text{molar}) - 13.07$ GPa. To examine the possible trend between the bulk modulus and molar volume among post-perovskite analos, we summarize the available data for oxide post-perovskites from experimental and theoretical investigations (Table 3). In Fig. 8, we plot the post-perovskite data in a diagram of K_T versus $1/V$ (molar). The bulk modulus of $CaIrO_3$, $MgGeO_3$ and (Mg, Fe)SiO_3 can be well characterized using the relationship $K_{T0} = 5{,}406.0/V(\text{molar}) + 5.9$ GPa (Fig. 8), with an RMS misfits of ~13 GPa. Recently, $CaRuO_3$, $CaRhO_3$, and $CaPtO_3$ are found to possess the $CaIrO_3$-type ppv structure at high pressure and/or high temperature, but no bulk moduli are available yet for these materials (Kojitani et al. 2007; Ohgushi et al. 2008; Shirako et al. 2009). Using the trend, obtained in this study, the bulk moduli of $CaRuO_3$, $CaPtO_3$, and $CaRhO_3$ ppv are predicted to be 167, 163, and 168 GPa, respectively, with estimated standard errors of ~6 GPa,. The standard error is determined using PROC GLM (procedure general linear model) of SAS (Statistical Analysis Software) program.

The bulk modulus K_{T0} and its temperature derivative $(\partial K_T/\partial T)_P$ for $CaIrO_3$ ppv obtained in this study show good consistency with the trend exhibited by other oxides and silicates as summarized in a previous study (see Fig. 9 of Duffy and Wang (1998)). In addition, an examination of the pressure derivatives of the bulk modulus K'_{T0} (Table 3) suggests that, excluding the fixed values ($K'_{T0} = 4$) and the study of Ballaran et al. (2007) ($K'_{T0} = 2.3$), all the K'_{T0} are greater than 4, indicating that the oxide post-perovskite may possess a pressure derivative larger than 4.

Conclusion

Using synchrotron X-radiation and a DIA-type cubic anvil apparatus, P–V–T measurements on $CaIrO_3$ post-perovskite have been carried out at pressures up to 8.6 GPa and

Table 3 Elasticity of oxide post-perovskites

References	Formula	V_0, Å^3	V_0, cm^3 M^{-1}	K_{T0}, GPa	K'_{T0}
This study	$CaIrO_3$	226.566	34.110	168.3	5.4
Lindsay-Scott et al. (2007)	$CaIrO_3$	226.402	34.085	144	4.8
Stølen and Trønnes (2007)[a]	$CaIrO_3$	233.22	35.111	164	4[b]
Martin et al. (2007)	$CaIrO_3$	226.3754	34.081	180.2	
Ballaran et al. (2007)	$CaIrO_3$	226.38	34.082	181	2.3
Usui et al. (2010)	$MgGeO_3$	182.2	26.979	185.0	4.314
Kubo et al. (2006)	$MgGeO_3$	179.2	27.430	207	4.4
Kubo et al. (2006)[a,c]	$MgGeO_3$	178.02	27.566	201.9	4.34
Hirose et al. (2005)	$MgGeO_3$	183.1	26.801	192	4[b]
Komabayashi et al. (2008)	$MgSiO_3$	163.813	24.662	223.2	4[b]
Guignot et al. (2007)	$MgSiO_3$	162.2	24.419	231.2	4[b]
Ono et al. (2006)	$MgSiO_3$	162.86	24.519	237.0	4[b]
Tsuchiya et al. (2005b)[c]	$MgSiO_3$		24.66	215.9	4.41
Tsuchiya et al. (2004)	$MgSiO_3$	163.813	24.662	222	4.2
Oganov and Ono (2004)[c]	$MgSiO_3$	162.86	24.519	231.93	4.430
Oganov and Ono (2004)[d]	$MgSiO_3$	167.64	25.238	199.96	4.541
Nishio-Hamane and Yagi (2009)	$(Mg_{0.9},Fe_{0.1})SiO_3$	164.1	24.705	224	4[b]
Nishio-Hamane and Yagi (2009)	$(Mg_{0.85},Fe_{0.15})(Al_{0.15}Si_{0.85})O_3$	166.5	25.067	220	4[b]
Shim et al. (2008)	$(Mg_{0.91},Fe_{0.09})SiO_3$	164.7	24.796	221	4[b]
Shieh et al. (2006)	$(Mg_{0.91},Fe_{0.09})SiO_3$	164.9	24.826	219	4[b]
Mao et al. (2006)	$(Mg_{0.6}Fe_{0.4})SiO_3$	157.2	23.666	272	6[b]
Kojitani et al. (2007)	$CaRuO_3$	223.34	33.624	167 (6)[e]	
Ohgushi et al. (2008)	$CaPtO_3$	227.942	34.317	163 (6)[e]	
Shirako et al. (2009)	$CaRhO_3$	222.03	33.427	168 (6)[e]	

[a] At 0 K

[b] Fixed

[c] Local density approximation (LDA)

[d] Generalized gradient approximation (GGA)

[e] Predicted values. Standard errors, in the brackets, are determined using PROC GLM (procedure general linear model) of SAS (Statistical Analysis Software) program

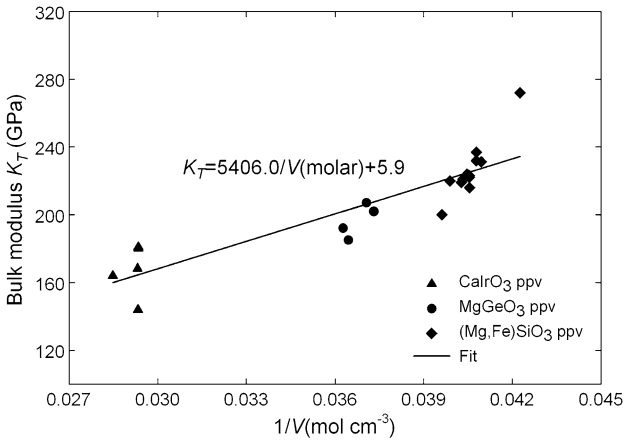

Fig. 8 Variation of bulk modulus K_{T0} with the molar volume V_0 (molar) for oxide post-perovskites. The *solid line* represents the relationship for isostructural oxide post-perovskites

temperatures from 298 to 1,273 K. A complete thermal equation of state has been derived by different equation of state approaches, namely the high-temperature Birch-Murnaghan equation of state, the thermal pressure approach, and the Mie-Grüneisen-Debye formalism. Both high-temperature Birch-Murnaghan EoS and thermal pressure approach gave consistent thermoelastic properties. To expand the pressure and temperature coverage, we combined previous data on $CaIrO_3$ post-perovskite at higher pressures or temperatures and performed an integrated analysis, yielding comparable results with those derived from the current data set alone. The derived bulk modulus K_{T0} at ambient pressure is 168.3 (71) GPa with a pressure derivative $K'_{T0} = 5.4$ (7). The refined thermoelastic parameters for $CaIrO_3$ post-perovskite (ppv) are temperature derivative of bulk modulus $(\partial K_T/\partial T)_P = -0.038$ (11) GPa K^{-1}, $\alpha K_T = 0.0039$

(1) GPa K^{-1}, $(\partial K_T/\partial T)_V = -0.012$ (2) GPa K^{-1}, and $\left(\partial^2 P/\partial T^2\right)_V = 1.9$ (3) $\times 10^{-6}$ GPa^2 K^{-2}. Using the Mie-Grüneisen-Debye formalism, we obtain Grüneisen parameter $\gamma_0 = 0.92$ (1) and its volume dependence $q = 3.4$ (6). A systematic relationship, $K_{T0} = 5{,}406.0/V(\text{molar}) + 5.9$ GPa, has been established for oxide post-perovskites.

Addendum

After the submission of the manuscript, Lindsay-Scott et al. (2010) reported an X-ray powder diffraction study on $CaPtO_3$ ppv using synchrotron radiation. The bulk modulus K_{T0} at ambient pressure and its pressure derivative K'_{T0} are determined to be 168.2 (8) GPa and 4.51 (6), respectively, from the third-order Birch–Murnaghan equation of state analysis. Using the trend $K_{T0} = 5{,}406.0/V(\text{molar}) + 5.9$ GPa derived in our study, $K_{T0}$of $CaPtO_3$ ppv has been predicted to be 163 (6) GPa (Table 3). The predicted value is in excellent agreement with the one derived from the experimental data within mutual uncertainty, indicating the validation of such trend for some ppv materials.

Acknowledgments We thank R. Cava and D. V. West (Princeton University) who provided assistance in sample synthesis. This work was supported by grants from NSF (EAR0635860) and DOE/NNSA (DEFG5209NA29458 to BL). The experiments were carried out at the National Synchrotron Light Source (NSLS), which is supported by the US Department of Energy, Division of Materials Sciences and Division of Chemical Sciences under Contract No. DE-AC02-76CH00016. The operation of X-17B2 is supported by COMPRES, the Consortium for Materials Properties Research in Earth Sciences. The sample used in this study was synthesized at GeoSoilEnviroCARS (Sector 13), Advanced Photon Source (APS), Argonne National Laboratory. GeoSoilEnviroCARS is supported by the National Science Foundation—Earth Sciences (EAR-0622171) and Department of Energy—Geosciences (DE-FG02-94ER14466). Use of the Advanced Photon Source was supported by the U. S. Department of Energy, Office of Science, Office of Basic Energy Sciences, under Contract No. DE-AC02-06CH11357. Mineral Physics Institute Publication No. 482.

References

Anderson OL (1984) A universal thermal equation-of-state. J Geodyn 1:185–214

Anderson OL (1995) Equation of state of solids for geophysics and ceramic science. Oxford Univ, Press, New York

Anderson OL (1999) The volume dependence of thermal pressure in perovskite and other minerals. Phys Earth Planet Inter 112(3–4): 267–283

Ballaran TB, Trønnes RG, Frost DJ (2007) Equations of state of $CaIrO_3$ perovskite and post-perovskite phases. Am Mineral 92(10):1760–1763

Bass JD (1984) Elasticity of single-crystal $SmAlO_3$, $GdAlO_3$ and $ScAlO_3$ perovskites. Phys Earth Planet Inter 36:145–156

Boehler R, Ramakrishnan J (1980) Experimental results on the pressure dependence of the Grüneisen parameter: A review. J Geophys Res 85:6996–7002

Caracas R, Cohen RE (2005) Effect of chemistry on the stability and elasticity of the perovskite and post-perovskite phases in the $MgSiO_3$-$FeSiO_3$-Al_2O_3 system and implications for the lowermost mantle. Geophys Res Lett 32:L06303

Debye P (1912) The theory of specific warmth. Annalen Der Physik 39:789–839

Decker DL (1971) High-pressure equation of state for NaCl, KCl, and CsCl. J Appl Phys 42:3239–3244

Duffy TS, Ahrens TJ (1995) Compressional sound velocity, equation of state, and constitutive response of shock-compressed magnesium oxide. J Geophys Res 100:529–542

Duffy TS, Wang YB (1998) Pressure-volume-temperature equations of state, in: Ultrahigh-pressure mineralogy-physics and chemistry of the Earth's deep interior. Rev Mineral 37:425–457

Guignot N, Andrault D, Morard G, Bolfan-Casanova N, Mezouar M (2007) Thermoelastic properties of postperovskite phase $MgSiO_3$ determined experimentally at core-mantle boundary *P–T* conditions. Earth Planet Sci Lett 256:162–168

Hernlund JW, Thomas C, Tackley PJ (2005) A doubling of the post-perovskite phase boundary and structure of the Earth's lowermost mantle. Nature 434:882–886

Hirose K, Fujita Y (2005) Clapeyron slope of the post-perovskite phase transition in $CaIrO_3$. Geophys Res Lett 32:L13313

Hirose K, Kawamura K, Ohishi Y, Tateno S, Sata N (2005) Stability and equation of state of $MgGeO_3$ post-perovskite phase. Am Mineral 90:262–265

Hunt SA, Weidner DJ, Li L, Wang LP, Walte NP, Brodholt JP, Dobson DP (2009) Weakening of calcium iridate during its transformation from perovskite to post-perovskite. Nature Geoscience 2:794–797

Hustoft J, Shim SH, Kubo A, Nishiyama N (2008) Raman spectroscopy of $CaIrO_3$ postperovskite up to 30 GPa. Am Mineral 93:1654–1658

Jackson I, Rigden SM (1996) Analysis of *P–V–T* data: Constraints on the thermoelastic properties of high-pressure minerals. Phys Earth Planet Inter 96:85–112

Kojitani H, Shirako Y, Akaogi M (2007) Post-perovskite phase transition in $CaRuO_3$. Phys Earth Planet Inter 165:127–134

Komabayashi T, Hirose K, Sugimura E, Nagayoshi S, Ohishi Y, Dubrovinsky LS (2008) Simultaneous volume measurements of post-perovskite and perovskite in $MgSiO_3$ and their thermal equation of state. Earth Planet Sci Lett 265:515–524

Kubo A, Kiefer B, Shen G, Prakapenka VB, Cava RJ, Duffy TS (2006) Stability and equation of state of the post-perovskite phase in $MgGeO_3$ to 2 Mbar. Geophys Res Lett 33:L12S12

Kubo A, Kiefer B, Shim S-H, Shen G, Prakapenka VB, Duffy TS (2008) Rietveld structure refinements of $MgGeO_3$ post-perovskite phase to 1 Mbar. Am Mineral 93:965–976

Kung J (1997) Systematics among the elastic properties of perovskite-structured compounds and geophysical implications. Australian National University. Ph.D thesis

Kung J, Li BS, Weidner DJ, Zhang JZ, Liebermann RC (2002) Elasticity of (Mg0.83, Fe0.17)O ferropericlase at high pressure: Ultrasonic measurements in conjunction with x-radiation techniques. Earth Planet Sci Lett 203:557–566

Larson AC, Von Dreele RB (2000) General Structure Analysis System (GSAS). Los Alamos National Laboratory Report LAUR 86–748

Lay T, Hernlund J, Garnero EJ, Thorne MS (2006) A post-perovskite lens and *D″* heat flux beneath the central pacific. Science 314:1272–1276

Le Bail A (2005) Whole powder pattern decomposition methods and applications-A retrospection. Powder Diffr 20:316–326

Li BS, Kung J, Liebermann RC (2004) Modem techniques in measuring elasticity of earth materials at high pressure and high temperature using ultrasonic interferometry in conjunction with

synchrotron X-radiation in multi-anvil apparatus. Phys Earth Planet Inter 143:559–574

Liebermann RC, Jones LA, Ringwood AE (1977) Elasticity of aluminate, titanate, stannate, and germanate compounds with the perovskite structure. Phys Earth Planet Inter 14:165–178

Lindsay-Scott A, Wood IG, Dobson DP (2007) Thermal expansion of $CaIrO_3$ determined by X-ray powder diffraction. Phys Earth Planet Inter 162:140–148

Lindsay-Scott A, Wood IG, Dobson DP, Vocadlo L, Brodholt JP, Crichton W, Hanfland M, Taniguchi T (2010) The isothermal equation of state of $CaPtO_3$ post-perovskite to 40 GPa. Phys Earth Planet Inter 182:113–118

Liu W, Li BS (2006) Thermal equation of state of $(Mg_{0.9}Fe_{0.1})_2SiO_4$ olivine. Phys Earth Planet Inter 157:188–195

Liu W, Kung J, Wang LP, Li BS (2008) Thermal equation of state of $CaGeO_3$ perovskite. Am Mineral 93:745–750

Mao WL, Shen GY, Prakapenka VB, Meng Y, Campbell AJ, Heinz DL, Shu JF, Hemley RJ, Mao HK (2004) Ferromagnesian postperovskite silicates in the D'' layer of the Earth. Proc Natl Acad Sci USA 101:15867–15869

Mao WL, Mao H, Prakapenka VB, Shu J, Hemley RJ (2006) The effect of pressure on the structure and volume of ferromagnesian post-perovskite. Geophys Res Lett 33:L12S02

Martin CD, Crichton WA, Liu HZ, Prakapenka V, Chen JH, Parise JB (2006) Phase transitions and compressibility of $NaMgF_3$ (neighborite) in perovskite- and post-perovskite-related structures. Geophys Res Lett 33:L11305

Martin CD, Chapman KW, Chupas PJ, Prakapenka V, Lee PL, Shastri SD, Parise JB (2007) Compression, thermal expansion, structure, and instability of $CaIrO_3$, the structure model of $MgSiO_3$ post-perovskite. Am Mineral 92:1048–1053

Metsue A, Carrez P, Mainprice D, Cordier P (2009) Numerical modeling of dislocations and deformation mechanisms in $CaIrO_3$ and $MgGeO_3$ post-perovskites-comparison with $MgSiO_3$ post-perovskite. Phys Earth Planet Inter 174:165–173

Miyagi L, Nishlyama N, Wang YB, Kubo A, West DV, Cava RJ, Duffy TS, Wenk HR (2008) Deformation and texture development in $CaIrO_3$ post-perovskite phase up to 6 GGa and 1300 K. Earth Planet Sci Lett 268:515–525

Miyajima N, Walte N (2009) Burgers vector determination in deformed perovskite and post-perovskite of $CaIrO_3$ using thickness fringes in weak-beam dark-field images. Ultramicroscopy 109:683–692

Miyajima N, Ohgushi K, Ichihara M, Yagi T (2006) Crystal morphology and dislocation microstructures of $CaIrO_3$: A TEM study of an analogue of the $MgSiO_3$ post-perovskite phase. Geophys Res Lett 33:L12302

Murakami M, Hirose K, Kawamura K, Sata N, Ohishi Y (2004) Post-perovskite phase transition in $MgSiO_3$. Science 304:855–858

Nishihara Y, Takahashi E, Matsukage KN, Iguchi T, Nakayama K, Funakoshi K (2004) Thermal equation of state of $(Mg_{0.91}Fe_{0.09})_2SiO_4$ ringwoodite. Phys Earth Planet Inter 143:33–46

Nishio-Hamane D, Yagi T (2009) Equations of state for postperovskite phases in the $MgSiO_3$–$FeSiO_3$–$FeAlO_3$ system. Phys Earth Planet Inter 175:145–150

Niwa K, Yagi T, Ohgushi K, Merkel S, Miyajima N, Kikegawa T (2007) Lattice preferred orientation in $CaIrO_3$ perovskite and post-perovskite formed by plastic deformation under pressure. Phys Chem Miner 34:679–686

Oganov AR, Ono S (2004) Theoretical and experimental evidence for a post-perovskite phase of $MgSiO_3$ in Earth's D'' layer. Nature 430:445–448

Oganov AR, Ono S (2005) The high-pressure phase of alumina and implications for Earth's D″ layer. Proc Natl Acad Sci USA 102:10828–10831

Ohgushi K, Matsushita Y, Miyajima N, Katsuya Y, Tanaka M, Izumi F, Gotou H, Ueda Y, Yagi T (2008) $CaPtO_3$ as a novel post-perovskite oxide. Phys Chem Miner 35:189–195

Ono S, Ohishi Y (2005) In situ X-ray observation of phase transformation in Fe_2O_3 at high pressures and high temperatures. J Phys Chem Solids 66:1714–1720

Ono S, Kikegawa T, Ohishi Y (2006) Equation of state of $CaIrO_3$-type $MgSiO_3$ up to 144 GPa. Am Mineral 91:475–478

Panning M, Romanowicz B (2004) Inferences on flow at the base of Earth's mantle based on seismic anisotropy. Science 303:351–353

Rodi F, Babel D (1965) Erdalkaliiridium (IV)-oxide: Kristallstruktur von CaIrO3. Z Anorg Allg Chem 336:17–23

Santillan J, Shim SH, Shen GY, Prakapenka VB (2006) High-pressure phase transition in Mn_2O_3: Application for the crystal structure and preferred orientation of the $CaIrO_3$ type. Geophys Res Lett 33:L15307

Saxena SK, Zhang J (1990) Thermochemical and *P–V–T* systematics of data on solids, examples: tungsten and MgO. Phys Chem Mineral 17:45–51

Shieh SR, Duffy TS, Kubo A, Shen G, Prakapenka VB, Sata N, Hirose K, Ohishi Y (2006) Equation of state of the postperovskite phase synthesized from a natural (Mg, Fe)SiO3 orthopyroxene. Proc Natl Acad Sci USA 103:3039–3043

Shim S-H, Duffy TS (2000) Constraints on the *P–V–T* equation of state of $MgSiO_3$ perovskite. Am Mineral 85:354–363

Shim S-H, Kubo A, Duffy TS (2007) Raman spectroscopy of perovskite and postperovskite of $MgGeO_3$ to 123 GPa. Earth Planet Sci Lett 260:166–178

Shim S-H, Catalli K, Hustoft J, Kubo A, Prakapenka VB, Caldwell WA, Kunz M (2008) Crystal structure and thermoelastic properties of $(Mg_{0.91}Fe_{0.09})SiO_3$ postperovskite up to 135 GPa and 2700 K. Proc Natl Acad Sci USA 105:7382–7386

Shirako Y, Kojitani H, Akaogi M, Yamaura K, Takayama-Muromachi E (2009) High-pressure phase transition of $CaRhO_3$ perovskite. Phys Chem Miner 36:455–462

Stixrude L, Bukowinski MST (1990) Fundamental thermodynamic relations and silicate melting with implications for the constitution of D′. J Geophys Res 95:19311–19325

Stølen S, Trønnes RG (2007) The perovskite to post-perovskite transition in $CaIrO_3$: Clapeyron slope and changes in bulk and shear moduli by density functional theory. Phys Earth Planet Inter 164:50–62

Sugahara M, Yoshiasa A, Yoneda A, Hashimoto T, Sakai S, Okube M, Nakatsuka A, Ohtaka O (2008) Single-crystal X-ray diffraction study of $CaIrO_3$. Am Mineral 93:1148–1152

Tateno S, Hirose K, Sata N, Ohishi Y (2006) High-pressure behavior of $MnGeO_3$ and $CdGeO_3$ perovskites and the post-perovskite phase transition. Phys Chem Miner 32:721–725

Toby BH (2001) EXPGUI, a graphical user interface for GSAS. J Appl Cryst 34:210–213

Tsuchiya T, Tsuchiya J (2007) Structure and elasticity of cmcm $CaIrO_3$ and their pressure dependences: ab initio calculations. Phys Rev B 76:144119

Tsuchiya T, Tsuchiya J, Umemoto K, Wentzcovitch RM (2004) Phase transition in $MgSiO_3$ perovskite in the Earth's lower mantle. Earth Planet Sci Lett 224:241–248

Tsuchiya J, Tsuchiya T, Wentzcovitch RM (2005a) Transition from the Rh_2O_3(II)-to-$CaIrO_3$ structure and the high-pressure-temperature phase diagram of alumina. Physi Rev B 72:020103

Tsuchiya J, Tsuchiya T, Wentzcovitch RM (2005b) Vibrational and thermodynamic properties of $MgSiO_3$ postperovskite. J Geophys Res 110:B02204

Usui Y, Tsuchiya J, Tsuchiya T (2010) Elastic, vibrational, and thermodynamic properties of $MgGeO_3$ postperovskite investigated by first principles simulation. J Geophys Res 115:B03201

Walte N, Heidelbach F, Miyajima N, Frost D (2007) Texture development and tem analysis of deformed $CaIrO_3$: Implications for the D'' layer at the core-mantle boundary. Geophys Res Lett 34:L08306

Wang YB, Weidner DJ, Guyot F (1996) Thermal equation of state of $CaSiO_3$ perovskite. J Geophys Res 101:661–672

Wang Y, Weidne D Jr, Meng Y (1998) Advances in equation of state measurements in SAM-85. In: Manghnani MH, Yagi T (eds) Properties of earth, planetary materials at high pressure, temperature. American Geophysical Union, Washington, DC, pp 365–372

Weidner DJ, Vaughan MT, Ko J, Wang Y, Liu X, Yeganeh-Haeri A, Pacalo RE, Zhao Y (1992) Characterization of stress, pressure and temperature in SAM85, a DIA type high pressure apparatus, In: Syonov Y, Manghnani MH, (eds), High-pressure research: application to earth and planetary sciences, Geophysical monograph 67, Terra Scientific Publishing Company and Am. Geophys. Union, Tokyo and Washington, DC, pp 13–17

Wookey J, Stackhouse S, Kendall JM, Brodholt J, Price GD (2005) Efficacy of the post-perovskite phase as an explanation for lowermost-mantle seismic properties. Nature 438:1004–1007

Yoshino T, Yamazaki D (2007) Grain growth kinetics of $CaIrO_3$ perovskite and post-perovskite, with implications for rheology of D'' layer. Earth Planet Sci Lett 255:485–493